used in systems that permit noninvasive imaging of tissue characteristics which are not identifiable by other techniques. The system design has gray level resolution of 256 levels and spatial resolution of 5×5 mm. Both of these resolutions are sufficient to provide necessary information for indicating the potential of microwave-induced thermoelastic imaging as a useful method for imaging biological tissues. The hybrid parallel/serial design yields good picture quality of reasonable cost, provided the object is quasi-stationary.

REFERENCES

[1] A. C. Kak, "Special issue on computerized medical imaging," *IEEE Trans. Biomed. Eng.*, vol. 28, pp. 49–234, 1981.

[2] G. L. Brownell, T. F. Budinger, P. C. Lanterbur, and P. L. McGreer, "Position tomography and nuclear magnetic resonance," *Science*, vol. 215, pp. 619–626, 1982.

[3] J. C. Lin, *Microwave Auditory Effects and Applications*. Springfield: Charles C. Thomas, 1978.

[4] R. G. Olsen, "Generation of acoustic images from the absorption of pulsed microwave energy," in *Acoustic Imaging*, vol. 11, J. P. Powers, Ed. New York: Plenum, 1982, pp. 53–59.

[5] R. G. Olsen and J. C. Lin, "Acoustic imaging of a model of a human hand using pulsed microwave irradiation," *Bioelectromagn.*, vol. 4, pp. 397–400, 1983.

[6] L. S. Gournay, "Conversion of electromagnetic to acoustic energy by surface heating," *J. Acoust. Soc. Am.*, vol. 40, no. 6, pp. 1322–1330, 1966.

[7] R. S. Cobbold, *Transducers for Biomedical Measurements: Principles and Applications*. New York: Wiley-Interscience 1974, pp. 170–174.

[8] Analog Devices, *Data Acquisition Data Book*. vol. 1, 1982, pp. 14–20.

[9] C. A. Vergers, *Handbook of Electrical Noise*. Blue Ridge, Summit: TAB, 1979.

[10] H. Taub and D. Schilling, *Principles of Communication Systems*. New York: McGraw-Hill, 1971.

James C. Lin was born in 1942 and received the B.S., M.S., and Ph.D. degrees in electrical engineering from the University of Washington in Seattle.

Presently, he is Head of the Department of Bioengineering at the University of Illinois at Chicago, where he also serves as a Professor of Bioengineering and of Electrical Engineering, and as Director of the College of Engineering Robotics and Automation Laboratory. He formerly held professorial appointments at Wayne State University in Detroit and the University of Washington. His publications have appeared in many journals and books, and include the book on *Microwave Auditory Effects and Applications* (Springfield: Thomas, 1978). He received an IEEE Transactions Prize Paper Award in 1976 and a National Research Service Award in 1982.

Professor Lin has been a scientific consultant to numerous private, state, and federal agencies. He is a member of the editorial board of *Bioelectromagnetics*, IEEE TRANSACTIONS ON MICROWAVE THEORY AND TECHNIQUES, *Journal of Microwave Power*, and *Journal of Environmental Pathology and Toxicology*. He has served on the IEEE Committee on Man and Radiation (COMAR), Robotics and Automation Council, IEEE/EMBS Committee on Biomedical Robotics (Chair), IEEE/MTT Committee on Biological Effects and Medical Applications (Chair), ANSI Subcommittee C95.4 (chaired its Dosimetry Working Group), and URSI/US National Committee of the National Academy of Science. He has been a member of the Board of Governors for the International Microwave Power Institute and the Board of Governors for the Bioelectromagnetics Society. He also served on the Governor's Task Force to Review Project Seafarer (Michigan) in 1976.

✤

Karen H. Chan photo and biography unavailable at time of publication.

Limitations of Imaging with First-Order Diffraction Tomography

MALCOLM SLANEY, STUDENT MEMBER, IEEE, AVINASH C. KAK, MEMBER, IEEE, AND LAWRENCE E. LARSEN, SENIOR MEMBER, IEEE

***Abstract*—In this paper, the results of computer simulations used to determine the domains of applicability of the first-order Born and Rytov approximations in diffraction tomography for cross-sectional (or three-dimensional) imaging of biosystems are shown. These computer simulations were conducted on single cylinders, since in this case analytical expressions are available for the exact scattered fields. The simulations establish the first-order Born approximation to be valid for objects where the product of the relative refractive index and the diameter of the cylinder is less than 0.35λ. The first-order Rytov approximation is valid with essentially no constraint on the size of the cylinder; however, the relative refractive index must be less than a few percent.**

We have also reviewed the assumptions made in the first-order Born and Rytov approximations for diffraction tomography. Further, we have reviewed the derivation of the Fourier Diffraction Projection Theorem, which forms the basis of the first-order reconstruction algorithms. We then show how this derivation points to new FFT-based implementations for the higher order diffraction tomography algorithms that are currently being developed.

Manuscript received October 12, 1983; revised March 9, 1984.

M. Slaney and A. C. Kak are with the School of Electrical Engineering, Purdue University, West Lafayette, IN 47907.

L. E. Larsen is with Microwaves Department, Walter Reed Army Institute of Research, Washington, DC 20012.

I. INTRODUCTION

DURING THE past ten years, the medical community has increasingly called on X-Ray computerized tomography (CT) to help make its diagnostic images. With

0018-9480/84/0800-0860$01.00 ©1984 IEEE

this increased interest has also come an awareness of the dangers of using ionizing radiation, and this, for example, has made X-Ray CT unsuitable for use in mass screening of the female breast. As a result, in recent years, much attention has been given to imaging with alternative forms of energy, such as low-level microwaves, ultrasound, and MR (magnetic-resonance). Ultrasonic B-scan imaging has already found widespread clinical applications; however, it lacks the quantitative aspects of ultrasonic computed tomography, which, in turn, can only be applied to soft tissue structures such as the female breast.

A necessary attribute of any form of radiation used for biological imaging is that it be possible to differentiate between different tissues on the basis of propagation parameters. It has already been demonstrated by Larsen and Jacobi [15] that this condition is satisfied by microwave radiation with the relative dielectric constant and the electric loss factor in the 1–10-GHz range. When used for tomography, a distinct feature of microwaves is that they allow one to reconstruct cross-sectional images of the molecular properties of the object. The dielectric properties of the water molecule dominate the interaction of microwaves and biological systems [13], [14], and thus by interrogating the object with microwaves it is possible to image, for example, the state of hydration of an object.

The past interest in microwave imagery has focused primarily on either the holographic, or the pulse-echo modes. In the holographic mode, most attention has focused on conducting targets in air, although there are exceptions as represented by the work of Yue *et al.* [27] wherein low-dielectric-constant slabs embedded in earth were imaged. The approach of Yue *et al.* is not applicable to the cross-sectional imaging of complicated three-dimensional objects, because of the underlying assumptions made regarding the availability of *a priori* information about the 'propagators' in a volume cell of the object. Another example of microwave imaging with holography is the work of Gregoris and Iizuka [6], wherein conductors and planar dielectric voids were holographically imaged inside flat dielectric layers. A reflection from the air–dielectric interface provided the reference beam. Again, this work is not particularly relevant for microwave imaging of biosystems since many important biological constituents are dielectrics dominated by water. When used in the pulse-echo mode, microwaves again possess limited usefulness due to the requirement that the object be in the far field of the transmit/receive aperture.

Tomography represents an attractive alternative to both holography and pulse-echo for cross-sectional (or three-dimensional) reconstruction of geometrically complicated biosystems, but there is a fundamental difference between tomographic imaging with X-rays and microwaves. X-rays, being nondiffracting, travel in straight lines, and therefore, the transmission data measures the line integral of some object parameter along straight lines. This makes it possible to apply the Fourier-slice theorem [22], which says that the Fourier transform of a projection is equal to a slice of the two-dimensional Fourier transform of the object.

On the other hand, when microwaves are used for tomographic imaging, the energy often does not propagate along straight lines. When the object inhomogeneities are large compared to a wavelength, energy propagation is characterized by refraction and multipath effects. Moderate amounts of ray bending induced by refraction can be taken into account by combining algebraic reconstruction algorithms [2] with digital ray tracing and ray linking algorithms [1].

When the object inhomogeneities become comparable in size to a wavelength, it is not appropriate to talk about propagation along lines or rays, and energy transmission must be discussed in terms of wavefronts and fields scattered by the imhomogeneities. In spite of these difficulties, it has been shown [5], [10], [18], [26] that with certain approximations a Fourier-slice-like theorem can be formulated. In [21], this theorem was called the Fourier Diffraction Projection Theorem. It may simply be stated as follows:

> When an object is illuminated with a plane wave as shown in Fig. 1, the Fourier transform of the forward scattered fields measured on a line perpendicular to the direction of propagation of the wave (line *TT* in Fig. 1) gives the values of the two-dimensional Fourier transform of the object along a circular arc as shown in the figure.

In Section III, we will review the proof of this theorem. In our review, we will show how the derivation of the theorem points to an FFT-based implementation of higher order Born and Rytov algorithms, which are currently under development by us and other researchers. *The Fourier Diffraction Projection Theorem is valid only when the inhomogeneities in the object are weakly scattering.*

According to the Fourier Diffraction Projection Theorem, by illuminating an object from many different directions and measuring the diffracted data, one can, in principle, fill up the Fourier space with the samples of the Fourier transform of the object over an ensemble of circular arcs and then reconstruct the object by Fourier inversion.

The above theorem forms the basis of the first-order diffraction tomography. The work of Mueller *et al.* [18] was initially responsible for focusing the attention of many researchers on this approach to cross-sectional and three-dimensional imaging, although from a purely scientific standpoint the technique owes its origins to the now-classic paper by Wolf [26], and a subsequent article by Iwata and Nagata [9].

As shown in the review in Section II, the algorithms for diffraction tomography are derived from the classical wave equation. The wave equation is a nonlinear differential equation that relates an object to the surrounding fields. To estimate a cross-sectional image of an object, it is necessary to find a linear solution to the wave equation and then to invert this relation between the object and the scattered field. The necessary approximations for this purpose limit the range of objects that can be successfully imaged to those that do not severely change the incident

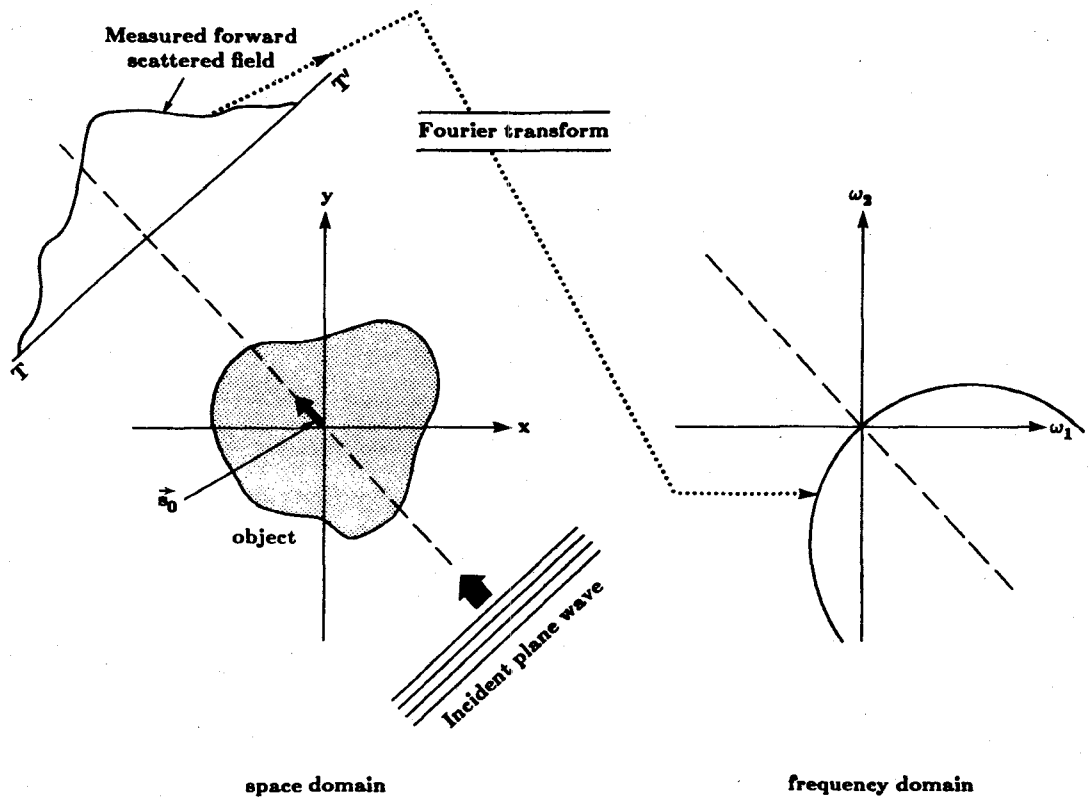

Fig. 1. The Fourier diffraction theorem.

field or have a small refractive index gradient compared to the surrounding media. In Section II, we will first review the two most common approximations used, the first-order Born and Rytov; and then in Section IV, we will show the effects of these approximations on computer-simulated reconstructions made from *exact* data.

These simulations will establish the first-order Born approximation to be valid for objects where the product of the change in refractive index and the diameter is less than 0.35λ, and the first-order Rytov approximation for changes in the refractive index of less than a few percent, with essentially no constraint on the object size.

II. Assumptions Underlying First-Order Diffraction Tomography

Diffraction tomography is based on a linear solution to the wave equation. The wave equation relates an object and the scattered field, and by linearizing it we can find an estimate of a cross section of the object based on the scattered field. The approximations used in the linearization process are crucial to the success of diffraction tomography, and we will be careful to highlight the assumptions.

In a homogeneous medium, electromagnetic waves satisfy a homogeneous wave equation of the form

$$\left(\nabla^2 + k_0^2\right)\psi(\vec{r}) = 0 \tag{1}$$

where the wavenumber k_0 represents the spatial frequency of the plane wave and is a function of the wavelength λ, or $k_0 = 2\pi/\lambda$. It is easy to verify that a solution to (1) is given by a plane wave

$$\psi(\vec{r}) = e^{j\vec{k}_0\cdot\vec{r}} \tag{2}$$

where $\vec{k}_0$ is the wave vector of the wave and satisfies the relation $|\vec{k}_0| = k_0$. For imaging, the interest is in an inhomogeneous medium, so the more general form of the wave equation is written as

$$\left(\nabla^2 + k(\vec{r})^2\right)\psi(\vec{r}) = 0. \tag{3}$$

For electromagnetic fields, if the effects of polarization are ignored, $k(\vec{r})$ can be considered to be a scalar function representing the refractive index of the medium. We then write

$$k(\vec{r}) = k_0 n(\vec{r}) = k_0\left[1 + n_\delta(\vec{r})\right] \tag{4}$$

where k_0 now represents the average wavenumber of the media, and $n(\vec{r})$ is the refractive index as given by

$$n(\vec{r}) = \sqrt{\frac{\mu(\vec{r})\epsilon(\vec{r})}{\mu_0\epsilon_0}}\,. \tag{5}$$

The parameter $n_\delta(\vec{r})$ represents the deviation from the average of the refractive index. In general, it will be assumed that the object of interest has finite support, so $n_\delta(\vec{r})$ is zero outside the object. Here, we have used μ and ϵ to represent the magnetic permeability and dielectric constant and the subscript zero to indicate their average values.

If the second-order terms in n_δ (i.e., $n_\delta \ll 1$) are ignored we find

$$(\nabla^2 + k_0^2)\psi(\vec{r}) = -2k_0^2 n_\delta(\vec{r})\psi(\vec{r}) = -\psi(\vec{r})O(\vec{r}) \quad (6)$$

where $O(\vec{r}) = 2k_0^2 n_\delta(\vec{r})$ is usually called the object function.

Note that (6) is a *scalar* wave propagation equation. Its use implies that there is no depolarization as the electromagnetic wave propagates through the medium. It is known [8] that the depolarization effects can be ignored only if the wavelength is much smaller than the correlation size of the inhomogeneities in the object. If this condition is not satisfied, then, strictly speaking, the following vector wave propagation equation must be used:

$$\nabla^2\vec{E}(r) + k_0^2 n^2 \vec{E}(\vec{r}) - 2\nabla\left[\frac{\nabla n}{n}\cdot\vec{E}\right] = 0 \quad (7)$$

where $\vec{E}$ is the electric-field vector. A vector theory for diffraction tomography based on this equation has yet to be developed.

In addition, $\psi_0(\vec{r})$, the incident field, is also defined as

$$(\nabla^2 + k_0^2)\psi_0(\vec{r}) = 0. \quad (8)$$

Thus, $\psi_0(\vec{r})$ represents the source field or the field present without any object inhomogeneities. The total field may be expressed as the sum of the incident field and the scattered field

$$\psi(\vec{r}) = \psi_0(\vec{r}) + \psi_s(\vec{r}) \quad (9)$$

with ψ_s satisfying the wave equation

$$(\nabla^2 + k_0^2)\psi_s(\vec{r}) = -\psi(\vec{r})O(\vec{r}) \quad (10)$$

which is obtained by substituting (8) and (9) in (6). This form of the wave equation will be used in the work to follow.

The scalar Helmholtz equation (10) cannot be solved for $\psi_s(\vec{r})$ directly, but a solution can be written in terms of a Green's function [16]. The Green's function, which is a solution of the differential equation

$$(\nabla^2 + k_0^2)G(\vec{r}|\vec{r}') = -\delta(\vec{r} - \vec{r}') \quad (11)$$

is written in 3-space as

$$G(\vec{r}|\vec{r}') = \frac{e^{jk_0 R}}{4\pi R} \quad (12)$$

with

$$R = |\vec{r} - \vec{r}'|. \quad (13)$$

In two dimensions, the solution of (11) is written in terms of a zero-order Hankel function of the first kind, and can be expressed as

$$G(\vec{r}|\vec{r}') = \frac{j}{4}H_0^{(1)}(k_0 R). \quad (14)$$

In both cases, the Green's function $G(\vec{r}|\vec{r}')$ is only a function of the difference $\vec{r} - \vec{r}'$, so the argument of the Green's function will often be represented as simply $G(\vec{r} - \vec{r}')$. Because the object function in (11) represents a point inhomogeneity, the Green's function can be considered to represent the field resulting from a single point scatterer.

Since (11) represents the radiation from a two-dimensional impulse source, the total radiation from all sources on the right-hand side of (11) must be given by the following superposition:

$$\psi_s(\vec{r}) = \int G(\vec{r} - \vec{r}')O(\vec{r}')\psi(\vec{r}')\,d\vec{r}'. \quad (15)$$

In general, it is impossible to solve (15) for the scattered field, so approximations must be made. Two types of approximations will be considered: the Born and the Rytov.

A. The Born Approximation

The Born approximation is the simpler of the two approaches. Consider the total field $\psi(\vec{r})$ expressed as the sum of the incident field $\psi_0(\vec{r})$, and a small perturbation $\psi_s(\vec{r})$ as in (9). The integral of (15) is now written as

$$\psi_s(\vec{r}) = \int G(\vec{r} - \vec{r}')O(\vec{r}')\psi_0(\vec{r}')\,dr' + \int G(\vec{r} - \vec{r}')O(\vec{r}')\psi_s(\vec{r}')\,dr'. \quad (16)$$

If the scattered field $\psi_s(\vec{r})$ is small compared to $\psi_0(\vec{r})$, the effects of the second integral can be ignored to arrive at the approximation

$$\psi_s(\vec{r}) = \int G(\vec{r} - \vec{r}')O(\vec{r}')\psi_0(\vec{r}')\,dr'. \quad (17)$$

This constitutes the first-order Born approximation. For a moment, let's denote the scattered fields obtained in this manner by $\psi_s^{(1)}(\vec{r})$. If one wished to compute $\psi_s^{(2)}(\vec{r})$, which represents the second-order approximation to the scattered fields, that could be accomplished by substituting $\psi_0 + \psi_s^{(1)}$ for ψ_0 in the right-hand side of (17), yielding

$$\psi_s^{(2)}(\vec{r}) = \int G(\vec{r} - \vec{r}')O(\vec{r}')\left[\psi_0(\vec{r}') + \psi_s^{(1)}(\vec{r}')\right]dr'. \quad (18)$$

In general, we may write

$$\psi_s^{(i+1)}(\vec{r}) = \int G(\vec{r} - \vec{r}')O(\vec{r}')\left[\psi_0(\vec{r}') + \psi_s^{(i)}(\vec{r}')\right]dr' \quad (19)$$

for the higher $(i+1)$th approximation to the scattered fields in terms of the ith solution. Since the science of reconstructing objects with higher order approximations is not fully developed, this particular point will not be pursued any further, and the first-order scattered fields will be represented by ψ_s (i.e., without the superscript).

Note again that the first-order Born approximation is valid only when the magnitude of the scattered field

$$\psi_s(\vec{r}) = \psi(\vec{r}) - \psi_0(\vec{r}) \quad (20)$$

is smaller than that of the incident field ψ_0. If the object is a cylinder of constant refractive index, it is possible to express this condition as a function of the size of the object (radius = a) and the refractive index. Let the incident wave

$\psi_0(\vec{r})$ be a plane wave propagating in the direction of the vector $\vec{k}_0$. For a large object, the field inside the object will not be given by

$$\psi(\vec{r}) = \psi_{\text{object}}(\vec{r}) \neq Ae^{j\vec{k}_0\cdot\vec{r}} \tag{21}$$

but instead will be a function of the change in refractive index n_δ. Along a ray through the center of the cylinder and parallel to the direction of propagation of the incident plane wave, the field inside the object becomes a slow (or fast) version of the incident wave or

$$\psi_{\text{object}}(\vec{r}) = Ae^{j(1+n_\delta)\vec{k}_0\cdot\vec{r}}. \tag{22}$$

Since the wave is propagating through the object, the phase difference between the incident field and the field inside the object is approximately equal to the integral of the change in refractive index through the object. Therefore, for a cylinder, the total phase shift through the object is approximately

$$\text{Phase Change} = 4\pi n_\delta \frac{a}{\lambda} \tag{23}$$

where λ is the wavelength of the incident wave. For the first-order Born approximation to be valid, a necessary condition is that the change in phase between the incident field and the wave propagating through the object be less than π. This condition can be expressed mathematically as

$$n_\delta a < \frac{\lambda}{4}. \tag{24}$$

B. The Rytov Approximation

The Rytov approximation is valid under slightly less severe restrictions. It is derived by considering the total field to be represented as [8]

$$\psi(\vec{r}) = e^{\phi(\vec{r})} \tag{25}$$

and rewriting the wave equation (1) as

$$(\nabla\phi)^2 + \nabla^2\phi + k_0^2 = -2k_0^2 n_\delta. \tag{26}$$

Expressing the total phase ϕ as the sum of the incident phase function ϕ_0 and the scattered complex phase ϕ_s or

$$\phi(\vec{r}) = \phi_0(\vec{r}) + \phi_s(\vec{r}) \tag{27}$$

where

$$\psi_0(\vec{r}) = e^{\phi_0(\vec{r})} \tag{28}$$

we find that

$$(\nabla\phi_0)^2 + 2\nabla\phi_0\cdot\nabla\phi_s + (\nabla\phi_s)^2 + \nabla^2\phi_0 + \nabla^2\phi_s + k_0^2(1+2n_\delta) = 0. \tag{29}$$

As in the Born approximation, it is possible to set the zero perturbation equation equal to zero to find

$$2\nabla\phi_0\cdot\nabla\phi_s + \nabla^2\phi_s = -(\nabla\phi_s)^2 - 2k_0^2 n_\delta. \tag{30}$$

This equation is inhomogeneous and nonlinear, but can be linearized by considering the following relation

$$\nabla^2(\psi_0\phi_s) = \nabla^2\psi_0\cdot\phi_s + 2\nabla\psi_0\cdot\nabla\phi_s + \psi_0\nabla^2\phi_s. \tag{31}$$

Recalling that

$$\psi_0 = Ae^{j\vec{k}_0\cdot\vec{r}} \tag{32}$$

we find

$$2\psi_0\nabla\phi_0\cdot\nabla\phi_s + \psi_0\nabla^2\phi_s = \nabla^2(\psi_0\phi_s) + k_0^2\psi_0\phi_s. \tag{33}$$

This result can be substituted into (30) to find

$$(\nabla^2 + k_0^2)\psi_0\phi_s = -\psi_0\left[(\nabla\phi_s)^2 + 2k_0^2 n_\delta\right]. \tag{34}$$

As before, the solution to this differential equation can again be expressed as an integral equation. This becomes

$$\psi_0\phi_s = \int_{V'} G(\vec{r}-\vec{r}')\psi_0\left[(\nabla\phi_s)^2 + 2k_0^2 n_\delta\right] dr' \tag{35}$$

where the Green's function is given by (14).

Under the Rytov approximation, it is assumed that the term in brackets in the above equation can be approximated by

$$(\nabla\phi_s)^2 + 2k_0^2 n_\delta \simeq 2k_0^2 n_\delta. \tag{36}$$

When this is done, the first-order Rytov approximation to the scattered phase ϕ_s becomes

$$\phi_s(\vec{r}) \simeq \frac{2}{\psi_0(\vec{r})}\int_{V'} G(\vec{r}-\vec{r}')\psi_0(\vec{r})k_0^2 n_\delta\, dr'. \tag{37}$$

Substituting the expression for ψ_s given in (17) yields

$$\phi_s(\vec{r}) \simeq \frac{\psi_s(\vec{r})}{\psi_0(\vec{r})}. \tag{38}$$

It is important to note that, in spite of the similarity of the Born (17) and the Rytov (37) solutions, the approximations are quite different. As will be seen later, the Born approximation produces a better estimate of the scattered **amplitude** for large deviations in the refractive index for objects small in size. On the other hand, the Rytov approximation gives a more accurate estimate of the scattered **phase** for large-sized objects with small deviations in refractive index.

When the object is small and the refractive index deviates only slightly from the surrounding media, it is possible to show that the Born and the Rytov approximations produce the same results. Consider our definition of the scattered phase in (25) and (27). Expanding the scattered phase in the exponential with the Rytov solution to the scattered field, it is seen

$$\psi(\vec{r}) = e^{\phi_0(\vec{r})+\phi_s(\vec{r})} = \psi_0(\vec{r})e^{\exp(-j\vec{k}_0\cdot\vec{r})\psi_s(\vec{r})}. \tag{39}$$

For very small $\psi_s(\vec{r})$, the first exponential can be written in terms of the power series expansion to find

$$\psi(\vec{r}) \simeq \psi_0(\vec{r})\left[1+\exp\left(-j\vec{k}_0\cdot\vec{r}\right)\psi_s(\vec{r})\right] = \psi_0(\vec{r}) + \psi_s(\vec{r}). \tag{40}$$

Thus, when the magnitude of the scattered field is very small, the Rytov approximation simplifies to the Born approximation.

The Rytov approximation is valid under a less restrictive set of conditions than the Born approximation [4], [11]. In

deriving the Rytov approximation, the assumption was made that

$$(\nabla\phi_s)^2 + 2k_0^2 n_\delta \simeq 2k_0^2 n_\delta. \tag{41}$$

Clearly this is true only when

$$n_\delta \gg \frac{(\nabla\phi_s)^2}{k_0^2}. \tag{42}$$

This can be justified by observing that, to a first approximation, the scattered phase ϕ_s is linearly dependent on n_δ [4]. If n_δ is small, then

$$(\nabla\phi_s)^2 \propto n_\delta^2 \tag{43}$$

will be even smaller, and, therefore, the first term in (41) above can be safely ignored. *Unlike the Born approximation, the size of the object is not a factor in the Rytov approximation.* The term $\nabla\phi_s$ is the change in the complex scattered phase per unit distance, and by substituting $k_0 = 2\pi/\lambda$, we find a necessary condition for the validity of the Rytov approximation is

$$n_\delta \gg \left[\frac{\nabla\phi_s \lambda}{2\pi}\right]^2. \tag{44}$$

Therefore, in the Rytov approximation, it is the change in scattered phase ϕ_s over one wavelength that is important and not the total phase. Thus, because of the ∇ operator, the Rytov approximation is valid when the phase change over a single wavelength is small.

III. Inversion of the Scattered Fields

The Fourier Diffraction Theorem relates the Fourier transform of the scattered field, the diffracted projection, to the Fourier transform of the object along a circular arc. While a number of researchers have derived this theory [18], [5], [21], [12], we would like to propose a system theoretic analysis of this result which is fundamental to first-order diffraction tomography. This approach is superior not only because it allows the scattering process to be visualized in the Fourier domain, but also because it points to efficient FFT-based computer implementations of higher order Born and Rytov algorithms currently under development. Since it appears that the higher order algorithms will be more computationally intensive, any savings in the computing effort involved is potentially important.

Consider the effect of a single plane wave incident on an object. The forward scattered field will be measured at a receiver line as shown in Fig. 2. We will find an expression for the field scattered by the object $O(\vec{r})$ by analyzing (17) in the Fourier domain. We will use the plots of Fig. 3 to illustrate the transformations that take place.

The first-order Born equation for the scattered field (17) can be considered as a convolution of the Green's function $G(\vec{r})$ and the product of the object function $O(\vec{r})$ and the incident field $\psi_0(\vec{r})$. First, we will define the following

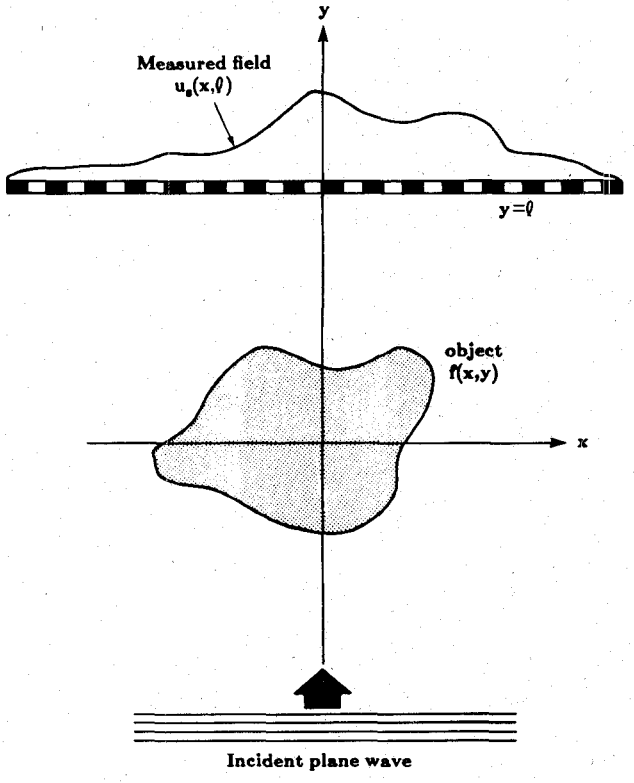

Fig. 2. A typical diffraction tomography experiment.

Fourier transform pairs:

$$O(\vec{r}) \leftrightarrow \tilde{O}(\vec{\Lambda})$$
$$G(\vec{r}) \leftrightarrow \tilde{G}(\vec{\Lambda}) \tag{45}$$

and

$$\psi(\vec{r}) \leftrightarrow \tilde{\psi}(\vec{\Lambda})$$

where we have used the relationships

$$\tilde{O}(\vec{\Lambda}) = \int\int O(\vec{r}) e^{-j\vec{\Lambda}\cdot\vec{r}}\, d\vec{r} \tag{46}$$

$\vec{\Lambda} = (\alpha, \beta)$ and (α, β) being the spatial frequencies along the x and y directions, respectively.

The integral solution to the wave equation (17) can now be written in terms of these Fourier transforms

$$\tilde{\psi}_s(\vec{\Lambda}) = \tilde{G}(\vec{\Lambda})\{\tilde{O}(\vec{\Lambda}) * \tilde{\psi}_0(\vec{\Lambda})\} \tag{47}$$

where we have used '$*$' to represent convolution. When the illumination field ψ_0 consists of a single plane wave

$$\psi_0(\vec{r}) = e^{j\vec{k}_0\cdot\vec{r}} \tag{48}$$

with $\vec{k}_0 = (k_x, k_y)$ satisfying the following relationship

$$k_0^2 = k_x^2 + k_y^2 \tag{49}$$

its Fourier transform is given by

$$\tilde{\psi}_0(\vec{\Lambda}) = 2\pi\delta(\vec{\Lambda} - \vec{k}_0). \tag{50}$$

The delta function causes the convolution of (47) to become a shift in the frequency domain as given by

$$\tilde{O}(\vec{\Lambda}) * \tilde{\psi}_0(\vec{\Lambda}) = 2\pi\tilde{O}(\vec{\Lambda} - \vec{k}_0). \tag{51}$$

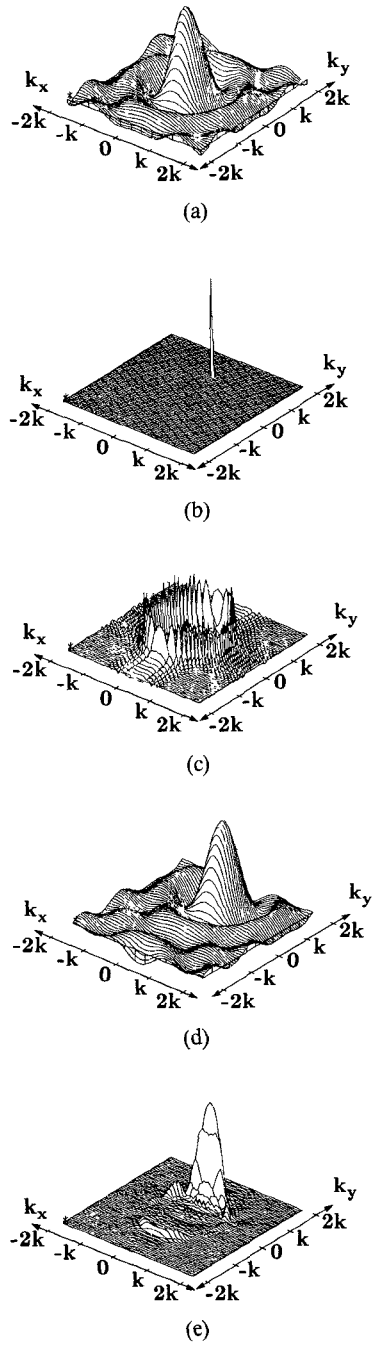

Fig. 3. Fourier spectrum representation of diffraction tomography experiment. (a) The object function, (b) the incident field, (c) the scattering potential, (d) the Green's function, and (e) the scattered field.

This convolution is illustrated in Fig. 3(a)–(c) for a plane wave propagating with direction vector $\vec{k}_0 = (0, k_0)$. Fig. 3(a) shows the Fourier transform of a single cylinder of radius 1λ, and Fig. 3(b) is the Fourier transform of the incident field. The resulting convolution in the frequency domain (or multiplication in the space domain) is shown in Fig. 3(c).

To find the Fourier transform of the Green's function, the Fourier transform of (11) is taken to find

$$\left(-\Lambda^2 + k_0^2\right)\tilde{G}\left(\vec{\Lambda}|\vec{r}'\right) = -e^{-j\vec{\Lambda}\cdot\vec{r}'} \tag{52}$$

where $\Lambda^2 = \alpha^2 + \beta^2$. Rearranging terms, we see that

$$\tilde{G}\left(\vec{\Lambda}|\vec{r}'\right) = \frac{e^{-j\vec{\Lambda}\cdot\vec{r}'}}{\Lambda^2 - k_0^2} \tag{53}$$

has a singularity for all $\vec{\Lambda}$ such that

$$\Lambda^2 = \alpha^2 + \beta^2 = k_0^2. \tag{54}$$

In the space domain, the two-dimensional Green's function, (14), has a singularity at the origin so it is necessary to approximate the function by using a two-dimensional average of the values near the singularity. An approximation to $\tilde{G}(\vec{\Lambda})$ is shown in Fig. 3(d).

The Fourier transform representation is misleading because it represents a point scatterer as both a sink and a source of waves. A single plane wave propagating from left to right can be considered in two different ways depending on the point-of-view. From the left side of the scatterer, the point scatterer represents a sink to the wave, while to the right of the scatterer the wave is spreading from a source point. Clearly, it is not possible for a scatterer to be both a point source and sink and later, when the expression for the scattered field is inverted, it will become necessary to choose a solution that leads to outgoing waves only.

The effect of the convolution shown in (17) is a multiplication in the frequency domain of the shifted object function, (51), and the Green's function, (53), evaluated at $\vec{r}' = 0$. The scattered field is written as

$$\tilde{\psi}_s(\vec{\Lambda}) = 2\pi \frac{\tilde{O}\left(\vec{\Lambda} - \vec{k}_0\right)}{\Lambda^2 - k_0^2}. \tag{55}$$

This result is shown in Fig. 3(e) for a plane wave propagating along the y axis. Since the largest frequency domain components of the Green's function satisfy (1), the Fourier transform of the scattered field is dominated by a shifted and sampled version of the object's Fourier transform.

We will now derive an expression for the field at the receiver line. For simplicity, it will be assumed that the incident field is propagating along the positive y axis or $\vec{k}_0 = (0, k_0)$. The scattered field along the receiver line $(x, y = l)$ is simply the inverse Fourier transform of the field in (55). This is written as

$$\psi_s(x, y = l) = \frac{1}{4\pi^2} \int\int \tilde{\psi}_s(\vec{\Lambda}) e^{j\vec{\Lambda}\cdot\vec{r}}\, d\alpha\, d\beta \tag{56}$$

which, using (55), can be expressed as

$$\psi_s(x, y = l) = \frac{1}{2\pi} \int\int \frac{\tilde{O}(\alpha, \beta - k_0)}{\alpha^2 + \beta^2 - k_0^2} e^{j(\alpha x + \beta l)}\, d\alpha\, d\beta. \tag{57}$$

We will carry out the integration with respect to β. For a given α, the integral has a singularity at

$$\beta_{1,2} = \pm\sqrt{k_0^2 - \alpha^2}. \tag{58}$$

Using contour integration, we can close the integration path at infinity and evaluate the integral with respect to β

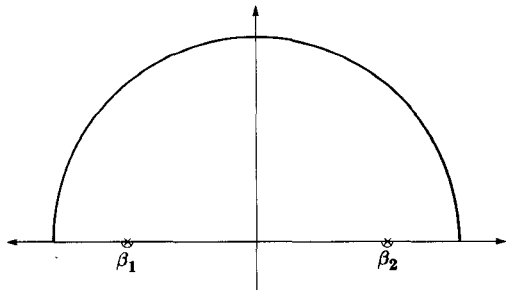

Fig. 4. Path of integration to calculate two-dimensional scattered fields.

along the path shown in Fig. 4 to find

$$\psi_s(x, y=l) = \int \Gamma_1(\alpha; l) e^{j\alpha x}\, d\alpha + \int \Gamma_2(\alpha; l) e^{j\alpha x}\, d\alpha \tag{59}$$

where

$$\Gamma_1 = \frac{\tilde{O}\left(\alpha, \sqrt{k_0^2 - \alpha^2} - k_0\right)}{j2\sqrt{k_0^2 - \alpha^2}} e^{j\sqrt{k_0^2 - \alpha^2}\, l} \tag{60}$$

and

$$\Gamma_2 = \frac{\tilde{O}\left(\alpha, -\sqrt{k_0^2 - \alpha^2} - k_0\right)}{-j2\sqrt{k_0^2 - \alpha^2}} e^{-j\sqrt{k_0^2 - \alpha^2}\, l}. \tag{61}$$

Examining the above pair of equations, it is seen that Γ_1 represents the solution in terms of plane waves traveling along the positive y axis while Γ_2 represents plane waves traveling in the $-y$ direction. In both cases, as α ranges from $-k_0$ to k_0, Γ represents the Fourier transform of the object along a semi-circular arc.

Since we are interested in the forward traveling waves, only the plane waves represented by the Γ_1 solution are valid, and thus the scattered field becomes

$$\psi_s(x, y=l) = \int \Gamma_1(\alpha; l) e^{j\alpha x}\, d\alpha, \qquad l > \text{object} \tag{62}$$

where we have chosen the value of the square root to lead only to outgoing waves.

Taking the Fourier transform of both sides of (62), we find that

$$\int \psi_s(x, y=l) e^{-j\alpha x}\, dx = \tilde{\Gamma}(\alpha, l). \tag{63}$$

But since $\Gamma(x, l)$ is equal to a phase-shifted version of the object function, the Fourier transform of the scattered field along the line $y = l$ is related to the Fourier transform of the object along a circular arc. The use of the contour integration is further justified by noting that only those waves that satisfy the relationship

$$\alpha^2 + \beta^2 = k_0^2 \tag{64}$$

will be propagated, and thus it is safe to ignore all waves not on the k_0-circle.

This result is diagramed in Fig. 5. The circular arc represents the locus of all points (α, β) such that $\beta = \pm\sqrt{k_0^2 - \alpha^2}$. The solid line shows the outgoing waves for a receiver line at $y = l$ greater than the object. This can be considered transmission tomography. Conversely, the dashed line indicates the locus of solutions for $y = l$ less than the object or the reflection tomography case.

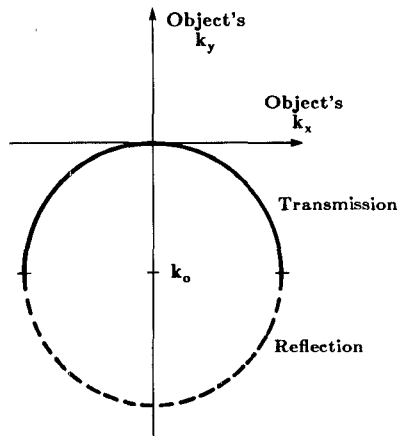

Fig. 5. The transmitted and reflected fields provide information about two different arcs in the object's Fourier domain.

Straight-ray (i.e., X-ray) tomography is based on the Fourier Slice Theorem [10], [22]

> The Fourier transform of a parallel projection of an image $f(x, y)$ taken at an angle θ gives a slice of the two-dimensional transform, $F(\omega_1, \omega_2)$ subtending an angle θ with the ω_1 axis.

This is diagramed in Fig. 6.

Equation (63) leads us to a similar result for diffraction tomography. Recall that α and β in (63) are related by

$$\beta = \sqrt{k_0^2 - \alpha^2}. \tag{65}$$

Thus, $\tilde{\Gamma}(\alpha)$, the Fourier transform of the received field, is proportional to $\tilde{O}(\alpha, \beta - k_0)$, the Fourier transform of the object along a circular arc. This result has been called the Fourier Diffraction Projection Theorem [21] and is diagramed in Fig. 1.

We have derived an expression, (63), that relates the scattering distribution of an object to the field received at a line. Within the diffraction limit, it is possible to invert this relation to estimate the object scattering distribution based on the received field.

A number of experimental procedures have been proposed to collect the data required to reconstruct the complete object. A single incident plane wave generates information along an arc in the object's Fourier domain, and by rotating the object [18], varying the frequency of the illuminating field [12], or by synthesizing an aperture [19], it is possible to fill up the Fourier space.

In addition, there are two types of algorithms that can be used to estimate the object. As proposed by Soumekh *et al.* [23], they can be described as interpolation in either the frequency or space domain. A comparison of these two methods has been published in [21].

The Fourier Diffraction Projection Theorem establishes a connection between the diffracted projections and an estimate of the object's Fourier transform along circular

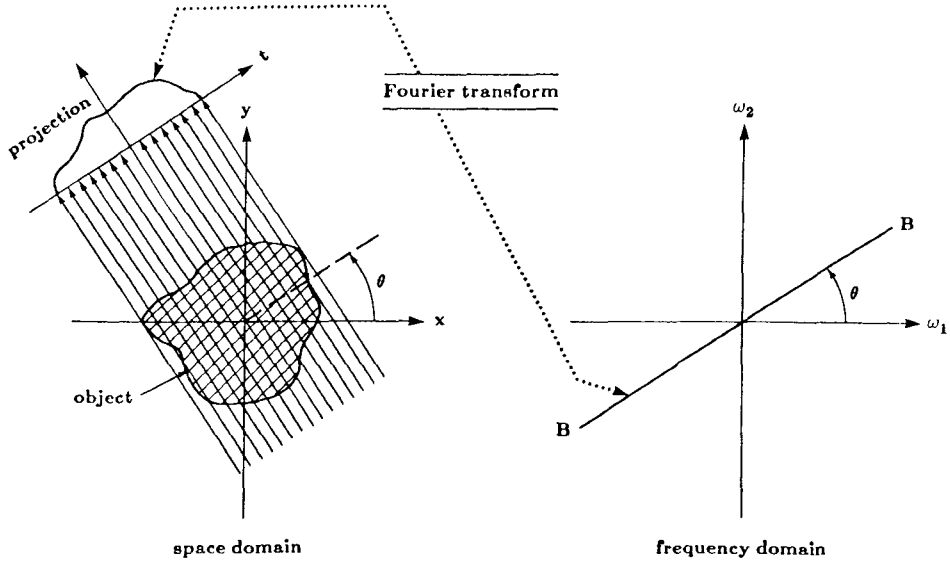

Fig. 6. The Fourier slice theorem.

arcs. The fact that the frequency domain samples are available over circular arcs, whereas, for fast Fourier inversion, it is desired to have samples over a rectangular lattice, is a source of computational difficulty with a direct Fourier inversion technique. Mueller *et al.* [17] have shown that by using nearest neighbor interpolation, it is possible to adequately map the data onto a rectangular grid and then use an FFT algorithm to invert the data. More sophisticated approaches are discussed in [21].

An interpolation procedure in the space domain was first proposed by A. J. Devaney [5]. This approach is similar to the backprojection algorithm [10] that made X-ray tomography successful, but since a propagation filter is applied to the projection data as it is smeared over the image plane, it has been called filtered-backpropagation. Since the propagation filter is depth-dependent, this approach is computationally more expensive than the frequency domain interpolation approach. It has been shown [21] that reconstructed images with bilinear interpolation are comparable in quality to those produced by filtered-backpropagation.

IV. Distortions Introduced by First-Order Algorithms

Several hundred computer simulations were performed to study the fundamental limitations of first-order diffraction tomography. In diffraction tomography, there are different approximations involved in the forward and inverse directions. In the forward process, it is necessary to assume that the object is weakly scattering so that either the Born or the Rytov approximations can be used. Once we arrive at an expression for the scattered field, it is necessary to not only measure the scattered fields but then numerically implement the inversion process.

The mathematical and experimental effects limit the reconstruction in different ways. The most severe mathematical limitations are imposed by the Born and the Rytov approximations. These approximations are fundamental to the reconstruction process and limit the range of objects that can be examined. On the other hand, the experimental limitations are caused because it is only possible to collect a finite amount of data. Up to the limit in resolution caused by evanescent waves, it is possible to improve a reconstruction by collecting more data.

By carefully setting up the simulations, it is possible to separate the effects of these errors. To study the effects of the Born and the Rytov approximations, it is necessary to calculate (or even measure) the exact fields and then make use of the best possible (most exact) reconstruction formulas available. The difference between the reconstruction and the actual object can then be used as a measure of the quality of the approximations.

These simulations are similar to a study performed by Azimi and Kak. In [3], the effects of multiple scattering on first-order diffraction tomography algorithms were discussed for objects consisting of multiple cylinders. It was concluded that even when object inhomogeneities are as small as 5 percent of the background, multiple scattering can introduce severe distortions in first-order reconstructions.

A. Qualitative Analysis

The exact field for the scattered field from a cylinder as shown by Weeks [25] was calculated for cylinders of various sizes and refractive index. In the simulations that follow, a single plane wave was incident on the cylinder, and the scattered field was calculated along a line at a distance of 100 wavelengths from the origin.

At the receiver line, the received wave was measured at 512 points spaced at 1/2 wavelength intervals. In all cases, the rotational symmetry of a single cylinder at the origin was used to reduce the computation time of the simulations.

The simulations were performed for refractive indices that ranged from 0.1-percent change (refractive index of 1.001) to a 20-percent change (refractive index of 1.2). For each refractive index, cylinders of size 1, 2, 4, and 10

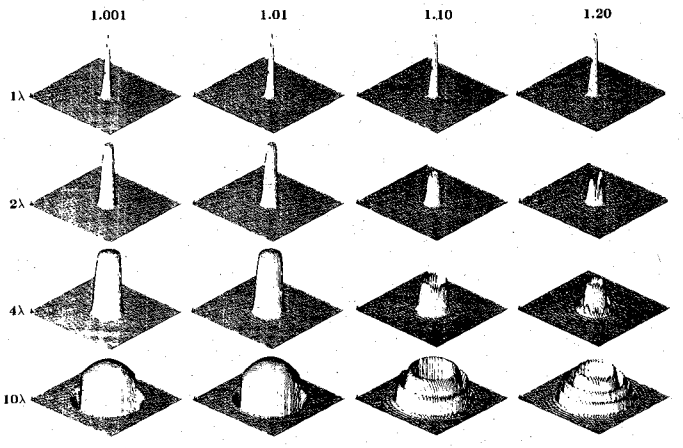

Fig. 7. Reconstructions using the Born approximation for cylinders of radius 1, 2, 4, and 10λ, and refractive indices of 1.001, 1.01, 1.10, and 1.20.

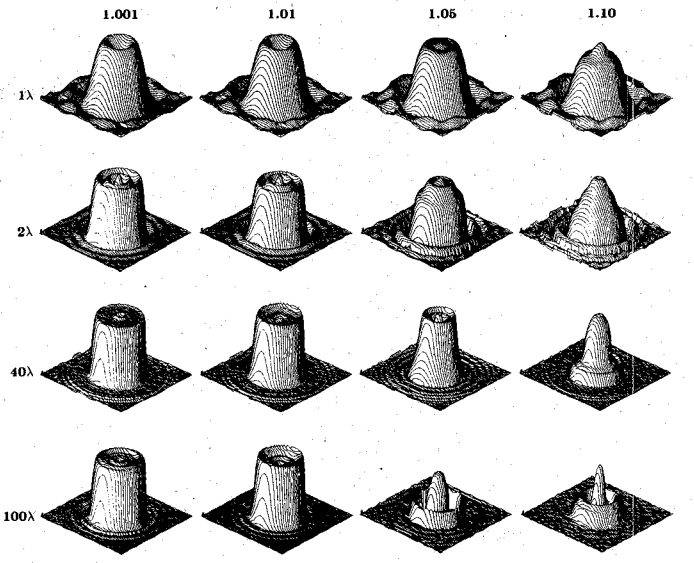

Fig. 8. Reconstructions using the Rytov approximation for cylinders of radius 1, 2, 40, and 100λ, and refractive indices of 1.001, 1.01, 1.05, and 1.10.

wavelengths were reconstructed. This gave a range of phase changes across the cylinder (see (23) above) from 0.004π to 8π. The resulting reconstructions using the Born approximation are shown in Fig. 7.

Clearly, all the cylinders of refractive index 1.001 in Fig. 7 were perfectly reconstructed. As (24) predicts, the results get worse as the product of refractive index and radius gets larger. The largest refractive index that was successfully reconstructed was for the cylinder in Fig. 7 of radius 1 wavelength and a refractive index that differed by 20 percent from the surrounding medium.

While it is hard to evaluate the two-dimensional reconstructions, it is certainly reasonable to conclude that only cylinders where the phase change across the object was less than or equal to 0.8π were adequately reconstructed. In general, the reconstruction for each cylinder where the phase change across the cylinder was greater than π shows severe artifacts near the center. This limitation in the phase change across the cylinder is consistent with the condition expressed in (24) above.

A similar set of simulations was also done for the Rytov approximation, and is shown in Fig. 8. In this case, the reconstructions were performed for cylinders of radius 1, 2, 40, and 100 λ, and refractive indices of 1.001, 1.01, 1.05, and 1.10. Because of the large variation in cylinder sizes, all reconstructions were performed so that the estimated object filled half of the reconstruction matrix. While the error in the reconstructions does increase for larger cylinders and higher refractive indices, it is possible to successfully reconstruct larger objects with the Rytov approximation.

B. Qualitative Comparison of the Born and Rytov Approximation

Reconstructions using exact scattered data show the similarity of the Born and Rytov approximations for small objects with small changes in the refractive index. For a cylinder of radius 1 wavelength and a refractive index that differs by 1 percent from the surrounding medium, the resulting reconstructions are shown in Fig. 9. In both cases,

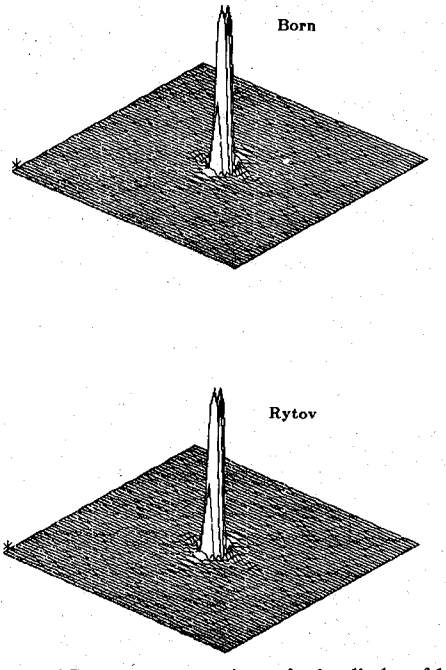

Fig. 9. Born and Rytov reconstructions of a 1 cylinder of 1λ radius and 1.01 refractive index.

the reconstructions are clean and the magnitude of the reconstructed change in refractive index is close to the simulated object.

On the other hand, the reconstructions of objects that are large or have a refractive index that differ by a large factor from one illustrate the differences between the Born and the Rytov approximations. Fig. 10 shows a simulated reconstruction for an object of radius 1 and refractive index of 1.20. In this region, the Born approximation is superior to the Rytov.

According to Chernov [4] and Keller [11], the Rytov approximation should be much superior to the Born for objects much larger than a wavelength. Reconstructions

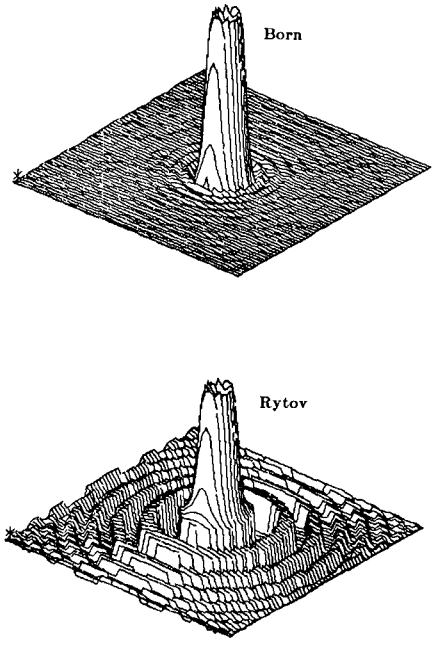

Fig. 10. Reconstructions of a radius 1λ cylinder and refractive index 1.20 showing the advantage of the Born over the Rytov.

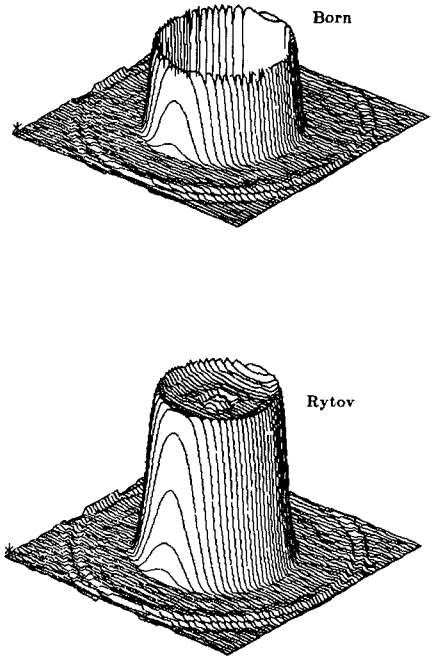

Fig. 11. Reconstructions of a radius 40λ cylinder and refractive index 1.01 showing the advantage of Rytov over the Born.

were done based on the exact scattered wave from a cylinder of radius 40 wavelengths and a refractive index that differed by 1 percent from the surrounding medium. The reconstructed refractive index is shown in Fig. 11. While the Born approximation has provided a good estimate of the size of the object, the reconstruction near the center is clearly not accurate.

The results in Figs. 10 and 11 are consistent with the regions of validity of the Born and Rytov approximations. The Born approximation is sensitive to the total phase shift in the object. Thus, in the reconstruction of Fig. 10, the Born approximation has done a good job of representing the step change in refractive index, but as the incident field undergoes a phase shift through the object, the reconstruction becomes poor. On the other hand, the Rytov approximation is sensitive to the change in refractive index. Thus, the Rytov reconstruction is accurate near the center of the object but provides a very poor reconstruction near the boundary of the object.

C. Quantitative Studies

In addition to the qualitative studies, a quantitative study of the error in the Born and Rytov reconstructions was also performed. As a measure of error, we used the relative mean squared error in the reconstruction of the object function integrated over the entire plane. If the actual object function is $O(\vec{r})$ and the reconstructed object function is $O'(\vec{r})$, then the relative Mean Squared Error (MSE) is

$$\text{MSE} = \frac{\int\int [O(\vec{r}) - O'(\vec{r})]^2 \, d\vec{r}}{\int\int [O(\vec{r})]^2 \, d\vec{r}}. \tag{66}$$

To study the quantitative difference between the Born and the Rytov approximations, several hundred simulated reconstructions were performed. For each simulation, the exact scattered field was calculated for a single cylinder with an arbitrary radius and refractive index. The reconstructions were divided into two sets to highlight the difference between the Born and the Rytov approximations.

The plots of Fig. 12 present a summary of the mean squared error for cylinders of 1, 2, and 3 λ in radius and twenty refractive indices between 1.01 and 1.20. In each case, the error for the Born approximation is shown as a solid line, while the error for the Rytov approximation is shown as a dashed line. The exact scattered fields were calculated at 512 receiver points along a receiver line 10λ from the center of the cylinder.

Only for the 1λ cylinders is the relative mean squared error for the Born approximation always lower than the Rytov. It is interesting to note that, while the Rytov approximation shows a steadily increasing error with higher refractive indices, the error in the Born reconstruction is relatively constant until a threshold is reached. For the 2λ and the 3λ cylinder, this breakpoint occurs at a phase shift of 0.6 and 0.7π. Thus, a criteria for the validity of the Born approximation is that the product of the radius of the cylinder in wavelengths and the change in refractive index must be less than 0.175.

Fig. 13 presents a summary of the relative mean squared errors for cylinders with refractive indices of 1.01, 1.02, and 1.03 and for forty radii between 1 and 40λ. Because the size of the cylinders varied by a factor of forty, the simulation parameters were adjusted accordingly. For a cylinder of radius R, the scattered field was calculated for 512 receivers along a line $2R$ from the center of the cylinder and spaced at $1/16R$ intervals.

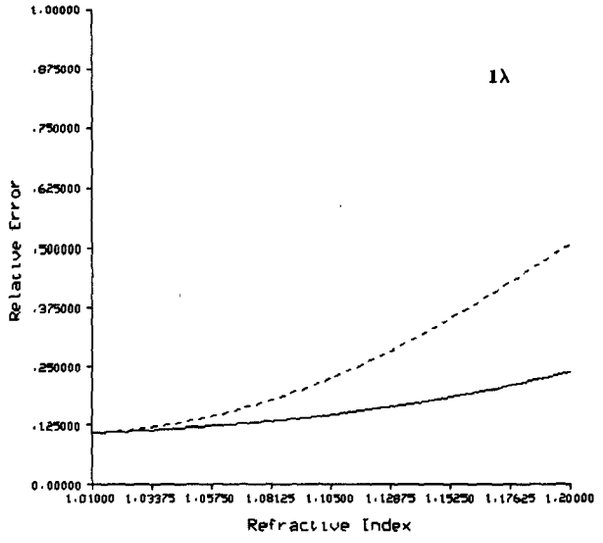

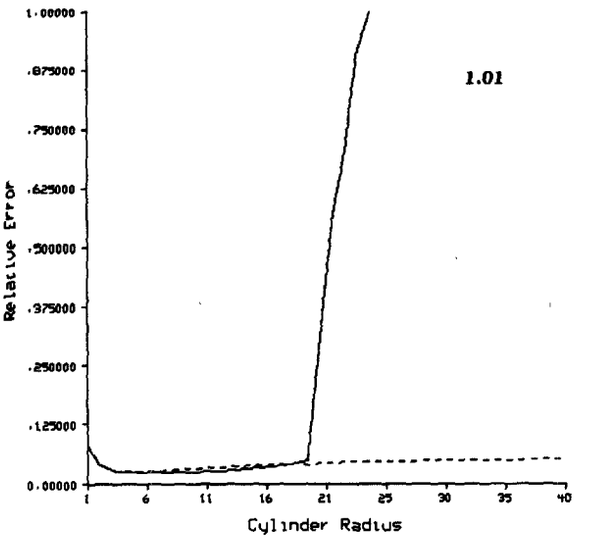

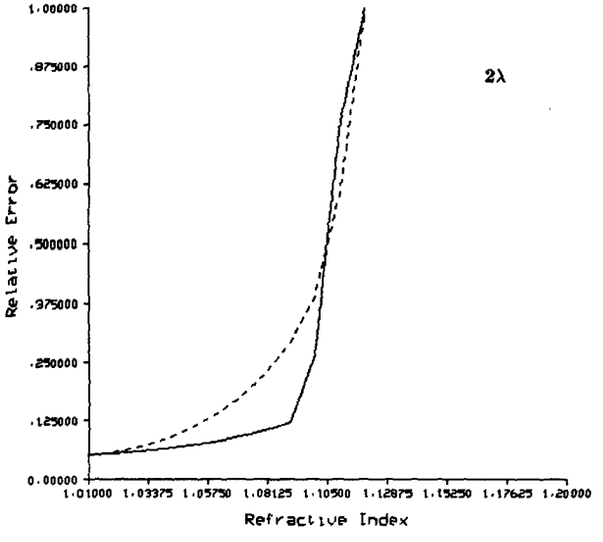

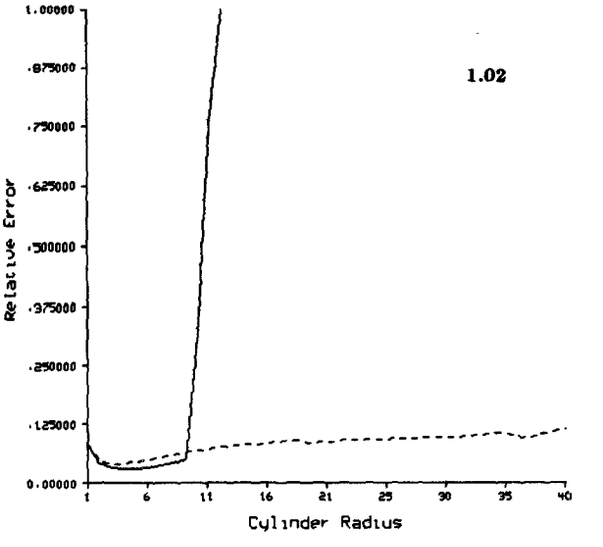

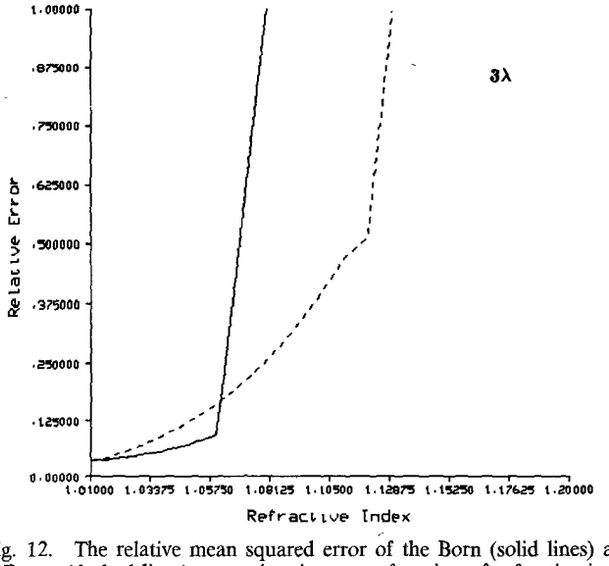

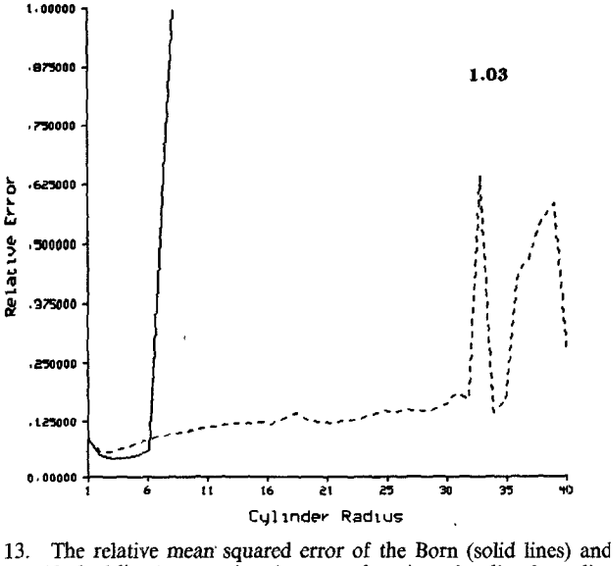

Fig. 12. The relative mean squared error of the Born (solid lines) and Rytov (dashed lines) approximations as a function of refractive index for cylinders of radius 1, 2, and 3λ.

Fig. 13. The relative mean squared error of the Born (solid lines) and Rytov (dashed lines) approximations as a function of radius for cylinders of refractive index 1.01, 1.02, and 1.03.

In each of the simulations, the Born approximation is only slightly better than the Rytov approximation until the Born approximation crosses its threshold with a phase shift of 0.7π. Because the error in the Rytov approximation is relatively flat, it is clearly superior for large object and small refractive indices. Using simulated data and the Rytov approximation, we have successfully reconstructed objects as large as 2000λ in radius.

D. Phase Error in the Born Approximation

The importance of the total phase shift of the incident field under the Born approximation was confirmed by considering the unwrapped phase of the reconstruction. Ho and Carter [7] proposed that the Born approximation actually reconstructs an estimate of the object function multiplied by the total field.

Recall the integral equation (15) which forms the basis of our reconstruction process:

$$\psi_s(\vec{r}) = \int O(\vec{r}')\psi_0(\vec{r}')G(\vec{r}-\vec{r}')\,d\vec{r}'. \tag{15}$$

An alternative to the Born approximation is to define

$$O'(\vec{r}) = \frac{O(\vec{r})\psi(\vec{r})}{\psi_0(\vec{r})} \tag{67}$$

and to substitute this modified object function $O'(\vec{r})$ for $O(\vec{r})$ in the integral of (17) above to find

$$\psi_s(\vec{r}) = \int O'(\vec{r}')\psi_0(\vec{r}')G(\vec{r}-\vec{r}')\,d\vec{r}'. \tag{17}$$

Since $\psi_0(\vec{r})$ and $G(\vec{r}-\vec{r}')$ are known exactly, for a single incident plane wave, the relationship between the scattered field and $O'(\vec{r})$ is exact. In practice, a tomographic image is formed using the information from multiple incident plane waves, and thus the reconstruction of $O'(\vec{r})$ can only provide approximate information about the failure of the Born approximation under large phase changes.

It is the relation between our exact estimate for $O'(\vec{r})$ and the actual object function $O(\vec{r})$ that we would like to investigate. Under the first Born approximation, we have assumed that

$$\psi_0(\vec{r}) \gg \psi_s(\vec{r}) \tag{68}$$

and thus to a good approximation

$$\psi(\vec{r}) \simeq \psi_0(\vec{r}). \tag{69}$$

Here

$$O'(\vec{r}) = \frac{O(\vec{r})\psi(\vec{r})}{\psi_0(\vec{r})} \simeq O(\vec{r}) \tag{70}$$

and thus our reconstruction procedure yields a good estimate of the object.

For objects that do not satisfy the Born approximation, part of the reconstruction error shows up as a phase shift. In (23), we estimated that a ray passing through the center of a homogeneous cylinder undergoes a phase shift of

$$\text{Phase Change} = \frac{4\pi n_\delta a}{\lambda}. \tag{23}$$

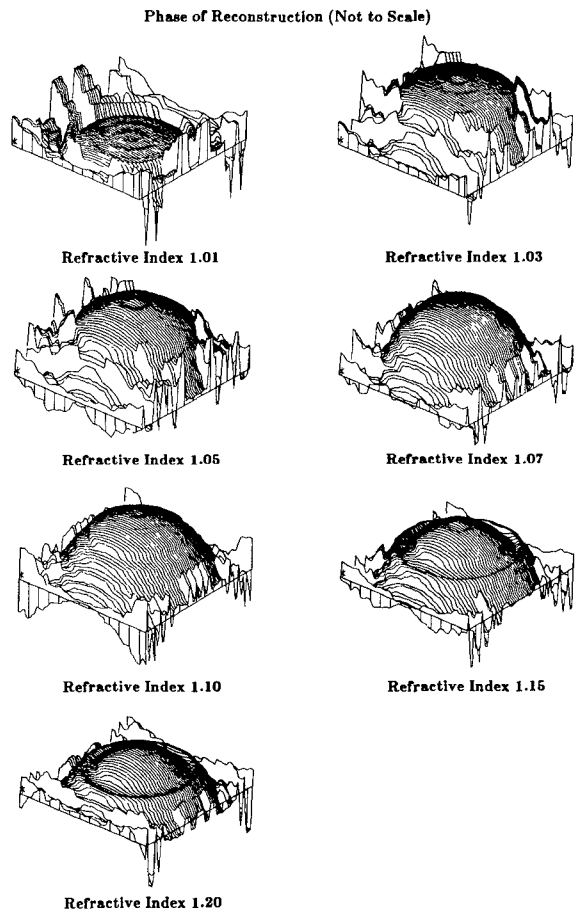

Fig. 14. Total unwrapped phase of the Born reconstruction for a 10λ cylinder with a refractive index between 1.01 and 1.20.

Thus, to a first approximation, the reconstruction of $O'(\vec{r})$ is related to the actual object function $O(\vec{r})$ by

$$O'(\vec{r}) = O(\vec{r})e^{j2\pi(n_\delta d/\lambda)} \tag{71}$$

where d represents the distance to the boundary of the object.

This approximate relationship was studied through a number of simulations. Fig. 14 shows the phase of the reconstruction of a cylinder with radius 10λ and refractive index that varied between 1.01 and 1.20. The phase of the reconstruction was unwrapped with a phase unwrapping algorithm proposed by Tribolet [24] and extended to two dimensions by O'Conner and Huang [20].

The total phase error at the center of a 10λ cylinder is shown in Fig. 15. While the total phase error does increase with refractive index at large refractive indices, it is apparent that a more complete theory is needed to estimate the object function more accurately.

V. Conclusions

By carefully designing a simulation procedure, we have isolated the effects of the first-order Born and Rytov approximations in diffraction imaging. While both procedures can produce excellent reconstructions for small objects with small refractive index changes, they both quickly break down when their assumptions are violated. The assumptions limit the Born approximation to objects where

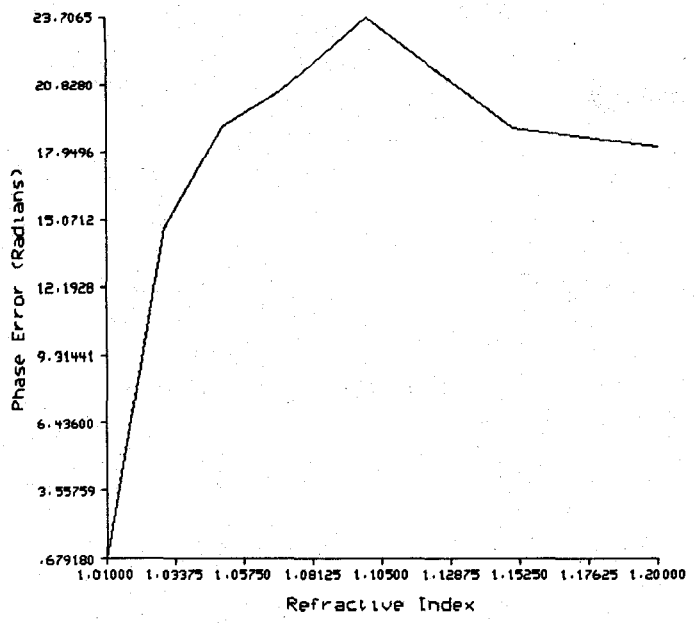

Fig. 15. Total unwrapped phase versus refractive index for a cylinder of radius 10λ.

the product of the diameter and the relative refractive index are less than 0.35λ and the Rytov approximation to objects with a refractive index that differ by less than 2 percent from the surrounding media, with essentially no constraint on the size of the object.

In addition, this paper has presented an alternative derivation of the Fourier Diffraction Projection Theorem. This approach will allow for efficient implementations of higher order reconstruction techniques on digital computers.

Several problems need to be solved for microwave imaging to become successful for medical imaging. Foremost, reconstruction algorithms based on higher order approximations to the scattered field will be needed. With 4-GHz microwaves in water, biological structures span tens of wavelengths and often have refractive index variations of 10 percent or more. In addition, high-frequency microwaves suffer from large attenuation in water-based systems, and an approach that takes into account the attenuation effects should be studied. Finally, the approach we have described here is only valid when the effects of depolarization can be ignored. For a complete solution, a Vector Diffraction Theorem will be needed.

REFERENCES

[1] A. H. Andersen and A. C. Kak, "Digital ray tracing in two-dimensional refractive fields," *J. Acoust. Soc. Am.*, vol. 72, pp. 1593–1606, Nov. 1982.

[2] ____, "Simultaneous algebraic reconstruction technique (SART): A superior implementation of the ART algorithm," *Ultrasonic Imaging*, to be published.

[3] M. Azimi and A. C. Kak, "Distortion in diffraction imaging caused by multiple scattering," *IEEE Trans. Med. Imaging*, vol. MI-2, pp. 176–195, Dec. 1983.

[4] L. A. Chernov, *Wave Propogation in a Random Medium*. New York: McGraw-Hill, 1960.

[5] A. J. Devaney, "A filtered backpropogation algorithm for diffraction tomography," *Ultrasonic Imaging*, vol. 4, pp. 336–350, 1982.

[6] Loris B. Gregoris and Keigo Iizuka, "Visualization of internal structure by microwave holography," *Proc. IEEE*, vol. 594, pp. 791–792, May 1970.

[7] P. C. Ho and W. H. Carter, "Structural measurement by inverse scattering in the first Born approximation," *Appl. Opt.*, vol. 15, pp. 313–314, Feb. 1976.

[8] A. Ishimaru, *Wave Propogation and Scattering in Random Media*. New York: Academic Press, 1978.

[9] K. Iwata and R. Nagata, "Calculation of refractive index distribution from interferograms using the Born and Rytov's approximations," *Jap. J. Appl. Phys.*, vol. 14, pp. 1921–1927, 1975.

[10] A. C. Kak, "Tomographic imaging with diffracting and non-diffracting sources," in *Array Processing Systems*, Simon Haykin, Ed. Englewood Cliffs, NJ: Prentice Hall, 1984.

[11] J. B. Keller, "Accuracy and validity of the Born and Rytov approximations," *J. Opt. Soc. Am.*, vol. 59, pp. 1003–1004, 1969.

[12] S. K. Kenue and J. F. Greenleaf, "Limited angle multifrequency diffraction tomography," *IEEE Trans. Sonics Ultrasonics*, vol. SU-29, pp. 213–217, July 1982.

[13] L. E. Larsen, J. H. Jacobi, and A. K. Krey, "Preliminary observations with an electromagnetic method for the noninvasive analysis of cell suspension physiology and induced pathophysiology," *IEEE Trans. Microwave Theory Tech.*, vol. MTT-26, pp. 581–595, Aug. 1978.

[14] L. E. Larsen and J. H. Jacobi, "Microwave interrogation of dielectric targets: Part 1: By scattering parameters," *Med. Phys.*, vol. 5, pp. 500–508, Nov./Dec. 1978.

[15] ____, "Microwave scattering parameter imagery of an isolated canine kidney," *Med. Phys.*, vol. 6, pp. 394–403, Sept./Oct. 1979.

[16] P. M. Morse and H. Feshbach, *Methods of Theoretical Physics*. New York: McGraw-Hill, 1953.

[17] R. K. Mueller, M. Kaveh, and R. D. Iversen, "A new approach to acoustic tomography using diffraction techniques," *Acoust. Imag.*, vol. 8, pp. 615–628, 1980.

[18] R. K. Mueller, M. Kaveh, and G. Wade, "Reconstructive tomography and applications to ultrasonics," *Proc. IEEE*, vol. 67, pp. 567–587, 1979.

[19] D. Nahamoo and A. C. Kak, "Ultrasonic diffraction imaging," School of Electrical Engineering, Purdue University, Tech. Rep. TR-EE-82-20, 1982.

[20] B. T. O'Connor and T. S. Huang, "Techniques for determining the stability of two-dimensional recursive filters and their application to image restoration," School of Electrical Engineering, Purdue University, Tech. Rep. TR-EE-78-18, pp. 6–24, May 1978.

[21] S. X. Pan and A. C. Kak, "A computational study of reconstruction algorithms for diffraction tomography: Interpolation vs. filtered backpropagation," *IEEE Trans. Acoust., Speech and Signal Processing*, pp. 1262–1275, Oct. 1983.

[22] A. Rosenfeld and A. C. Kak, *Digital Picture Processing*, 2nd ed. New York: Academic Press, 1982.

[23] M. Soumekh, M. Kaveh, and R. K. Mueller, "Algorithms and experimental results in acoustic tomography using Rytov's approximation," in *ICASSP 83 Proc.*, Apr. 1983, pp. 135–138.

[24] J. M. Tribolet, "A new phase unwrapping algorithm," *IEEE Trans. Acoust., Speech and Signal Processing*, vol. ASSP-25, pp. 170–177, Apr. 1977.

[25] W. L. Weeks, *Electromagnetic Theory for Engineering Applications*. New York: Wiley, 1964.

[26] E. Wolf, "Three-dimensional structure determination of semi-transparent objects form holographic data," *Opt. Communicat.*, vol. 1, pp. 153–156, 1969.

[27] O. C. Yue, E. L. Rope, and G. Tricoles, "Two reconstruction methods for microwave imaging of buried dielectric anomalie," *IEEE Trans. Computers*, vol. C-24, pp. 381–390, Apr. 1975.

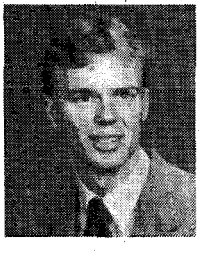

Malcolm Slaney (M'83) is completing his Ph.D. work at Purdue University, West Lafayette, IN, in the area of microwave and ultrasound tomography. He has been a Research Associate at Purdue from 1981 to 1984 and has worked on problems in computerized tomography, diffraction tomography, and depth perception for robotics.

Prior to joining Purdue, he worked for Bell Laboratories in the areas of switching systems software, fault tolerant computing, and

high-speed digital networks. Over the past few years, he also has consulted with several companies in the areas of digital control systems, X-ray tomography, and doppler ultrasound.

Mr. Slaney is a member of ACM and Eta Kappa Nu.

✤

Avinash C. Kak (M'71) is currently a Professor of Electrical Engineering at Purdue University, West Lafayette, IN. His current research interests are in computed imaging, image processing, and artificial intelligence. He has coauthored *Digital Picture Processing*, vols. 1 and 2 (New York: Academic), a second edition of which was published in 1983. He is an Associate Editor of *Computer Vision, Graphics and Image Processing* (New York: Academic), and *Ultrasonic Imaging* (New York: Academic). He was also a Guest Editor of the February 1981 Special Issue on Computed Imaging of the IEEE TRANSACTIONS ON BIOMEDICAL ENGINEERING. During the last ten years, he has consulted in the areas of computed imaging for many industrial and governmental organizations.

✤

Lawrence E. Larsen (M'81–SM'82) attended and received the M.D. degree magna cum laude from the University of Colorado, Fort Collins, in 1968. He was awarded an NIH postdoctoral fellowship in biophysics at UCLA for the period 1968–1970.

He then served in the United States Army as a Research Physiologist in the Department of Microwave Research at the Walter Reed Army Institute of Research during 1970–1973. From 1973 to 1975, he accepted a faculty appointment in the Radiology Department at the Baylor College of Medicine in Houston, TX, where he taught physiology and computer sciences. In 1975, he returned to the Walter Reed Army Institute of Research as the Associate Chief of Microwave Research. He was appointed the Department Chief in 1977 and presently serves in that role with the rank of Colonel, Medical Corps. He holds several patents.

Hyperthermia and Inhomogeneous Tissue Effects Using an Annular Phased Array

PAUL F. TURNER

Abstract—**A regional hyperthermia Annular Phased Array (APA) applicator is described, and examples of its various heating patterns, obtained by scanning the electric fields with a small E-field sensor, are illustrated. Also shown are the effects of different frequencies of an elliptical phantom cylinder having a 1-cm-thick artificial fat wall and the general dimensions of the human trunk. These studies show the APA's ability to achieve uniform heating at lower frequencies (below 70 MHz) or to focus central heating at moderately higher frequencies (above 70 MHz). The influence of human anatomical contours in altering heating patterns is discussed using results obtained with a female mannequin having a thin latex shell filled with tissue-equivalent phantom. Field perturbations caused by internally embedded low-dielectric structures are presented, showing the localized effects of small objects whose surfaces are perpendicular to the electric field.**

I. INTRODUCTION

ELECTROMAGNETIC (EM) hyperthermia has been clinically tested, for the most part, with superficial tumors in which the response is easily measured. Results obtained in these clinical trials corroborate findings from earlier *in vivo* and *in vitro* experiments that show this technique to be capable of selectively treating cancerous tumors. Much of the real potential of hyperthermia, however, lies in its ability to treat deep-seated localized tumors for which surgical removal is not a feasible solution. Such tumors have consistently presented one of the most difficult challenges facing both oncologists and technical researchers.

In response to this need, BSD Medical Corporation has developed an EM Annular Phased Array, or APA (patent pending), shown in Fig. 1, which has undergone testing since 1979 and which, during that time, has been shown to be capable of transmitting heating power directly to central body tissues [1]. The interaction of the human body and the EM field generated by the APA has been studied with phantom models [2], anesthetized laboratory animals [1], [3], and terminally ill human cancer patients [4], [5]. Results obtained in these trials show that deep regional hyperthermia is not only possible, but effective in controlling solid tumors in the center of the body. (Actual clinical application of this method is still restricted, primarily

Manuscript received October 12, 1983; revised March 8, 1984.

The author is with BSD Medical Corporation, 420 Chipeta Way, Suite 220, Salt Lake City, UT 84108.

0018-9480/84/0800-0874$01.00 ©1984 IEEE